6. T. D. Brock and J. Gustafson, *Appl. Environ. Microbiol.* **32**, 567 (1976); D. R. Boone *et al.*, *Int. J. Syst. Bacteriol.* **45**, 441 (1995); .A. Slobodkin *et al.*, *Doklady Akad. Nauk* **345**, 694 (1995); C. Zhang *et al.*, *Appl. Biochem. Biotechnol.* **57/58**, 923 (1996); A. C. Greene, B. K. C. Patel, A. J. Sheehy, *Int. J. Syst. Bacteriol.* **47**, 505 (1997); A. Slobodkin, A.-L. Reysenbach, N. Strutz, M. Dreier, J. Wiegel, *ibid.*, p. 541.
7. K. O. Stetter, G. Fiala, G. Huber, R. Huber, A. Segerer, *FEMS Microbiol. Rev.* **75**, 117 (1990); K. O. Stetter, *ibid.* **18**, 149 (1996).
8. H. Ohmoto and R. P. Felder, *Nature* **328**, 244 (1987); J. F. Kasting and T. P. Ackerman, *Science* **234**, 1383 (1986); J. F. Kasting, *Precamb. Res.* **34**, 205 (1987); *Science* **259**, 920 (1993).
9. D. L. Balkwill *et al.*, *Eos* **75**, 390 (1994); H.-Y. Tseng, T. C. Onstott, R. C. Burruss, D. S. Miller, *Chem. Geol.* **127**, 297 (1996); J. K. Pitman, W. W. Dickinson, in *U.S. Geological Survey Bulletin*, No. 1886 (1986), pp. J1–J15; R. C. Johnson, D. D. Rice, *Bull. Am. Assoc. Petrol. Geol.* **74**, 805 (1990).
10. Original enrichment cultures were initiated by inoculating samples at a 1:10 ratio into a basal medium [C. Zhang *et al.*, *Appl. Biochem. Biotechnol.* **57/58**, 923 (1996)] containing 1% (wt/v) NaCl, 70 mM amorphous Fe(III)-oxyhydroxide as an electron acceptor, and 10 mM of a short-chain fatty acid (formate, acetate, lactate, or pyruvate) or 80% H_2 (balanced with 20% CO_2 and at 1 atm. gas pressure) as an electron donor. The incubations were at 60°C (in the dark without shaking).
11. J. C. G. Walker, *Nature* **329**, 710 (1987); A. F. Trendall and R. C. Morris, Eds., *Iron-Formation: Facts and Problems* (Elsevier, Amsterdam, 1983); P. B. McMahon and F. H. Chapelle, *Nature* **349**, 233 (1991); B. N. Bjornstad *et al.*, *Ground Water Monitoring Remediation* **14**, 140 (1994).
12. R. G. Arnold, T. J. DiChristina, M. R. Hoffmann, *Appl. Environ. Microbiol.* **52**, 281 (1986); C. R. Myers and K. H. Nealson, *J. Bacteriol.* **172**, 6232 (1990); C. R. Myers and J. M. Myers, *FEMS Microbiol. Lett.* **108**, 15 (1993); *J. Appl. Bacteriol.* **76**, 253 (1994); Y. A. Gorby and D. R. Lovley, *Appl. Environ. Microbiol.* **57**, 867 (1991).
13. S. M. Barns, R. E. Fundyga, M. W. Jeffries, N. R. Pace, *Proc. Natl. Acad. Sci. U.S.A.* **91**, 1609 (1994); D. M. Ward, M. M. Bateson, R. Weller, A. L. Ruff-Roberts, *Adv. Microb. Ecol.* **12**, 219 (1992); J. A. Fuhrman, K. McCallum, A. A. Davis, *Nature* **356**, 148 (1992).
14. Genomic DNAs were extracted from the cells harvested from the enrichment cultures by means of the freezing-thawing and SDS lysis methods [J.-Z. Zhou *et al.*, *Appl. Environ. Microbiol.* **62**, 461 (1996)]. The 16*S* rRNA genes were amplified and cloned into the pCR™II TA cloning vector. The 16*S* rRNA gene inserts were detected by RFLP analysis with four tetrameric restriction enzymes: Msp I plus Rsa I and Hha I plus Hae III.
15. The 16*S* rRNA genes were partially sequenced with the reverse primer spanning *E. coli* 16*S* rRNA gene positions of 529–512 by means of an automatic fluorescent sequencer [J.-Z. Zhou *et al.*, *Int. J. Syst. Bacteriol.* **45**, 500 (1995)]. The phylogenetic tree was constructed by the maximum likelihood method with the program fastDNAml in EDP [N. Larsen *et al.*, *Nucleic Acids Res.* **21**, 3021 (1993)].
16. D. R. Boone, W. B. Whitman, P. Rouviere, In *Methanogenesis: Ecology, Physiology, Biochemistry, and Genetics*, J. G. Ferry, Ed. (Chapman & Hall, New York, 1993), pp. 35–80; N. K. Fry, S. Warwick, N. A. Saunders, T. M. Embley, *J. Gen. Microbiol.* **137**, 1215 (1991); R. Devereux *et al.*, *J. Bacteriol.* **172**, 3609 (1990); F. E. Dewhirst, B. J. Paster, I. Olsen, G. J. Fraser, *ibid.* **174**, 2002 (1992).
17. C. R. Woese, *Microbiol. Rev.* **51**, 221 (1987); C. R. Woese, O. Kandler, M. L. Wheelis, *Proc. Natl. Acad. Sci. U.S.A.* **87**, 4576 (1990).
18. L. P. Knauth and S. Epstein, *Geochim. Cosmochim. Acta* **40**, 1095 (1976); L. P. Knauth and D. R. Lowe, *Earth Planet. Sci. Lett.* **41**, 209 (1978); B. L. Winter and L. P. Knauth, *Precamb. Res.* **59**, 283 (1992).
19. D. S. McKay *et al.*, *Science* **273**, 924 (1996).
20. S. W. Squyres and J. F. Kasting, *ibid.* **265**, 744 (1994).
21. Fe(III) reduction was monitored by measuring the accumulation of Fe(II) by the ferrozine method [C. Zhang *et al.*, *Appl. Biochem. Biotechnol.* **57/58**, 923 (1996)]. Formation of magnetic minerals was visually inspected with a magnet and was confirmed by x-ray diffraction.
22. Slides for scanning electron microscopy were made by transferring undisturbed solid material to the poly-L-lysine–coated cover glass and fixed with 2.5% (by volume) glutaraldehyde (1 hour) and 2% $KMnO_4$ (30 min) at room temperature. The samples were then dehydrated with an ethanol series under aerobic conditions, air-dried, and coated with gold-palladium.
23. The *d*-spacings at 2.53 Å, 1.48 Å, 2.98 Å, 4.88 Å, 2.10 Å, and 1.71 Å and their intensities are shared by both magnetite (Fe_3O_4) and maghemite (the γ-Fe_2O_3 spinel) within the resolution limits of the electron diffraction technique. The *d*-spacings at 7.1 Å, 3.57 Å, and 2.78 Å are characteristic of maghemite.

24. We thank D. Coffey (ORNL; scanning electron microscopy), E. Voelkl (ORNL; transmission electron microscopy), W. R. Dunham and N. Moon (Univ. of Michigan; Mössbauer spectroscopy) for collaborative efforts, and A. V. Palumbo (ORNL) for discussion. Supported by the Subsurface Science Program managed by F. J. Wobber and the Geosciences Research Program of U.S. Department of Energy contracted to Lockheed Martin Energy Research Corp.; the ORNL Postdoctoral Research Associates Program administered jointly by ORNL and Oak Ridge Institute for Science and Education (S. V. Liu, J. Zhou, and C. Zhang); the ORNL Laboratory-Directed Research and Development Program; and the ORNL High-Temperature Materials Laboratory summer faculty fellowship program (M.G.J.).

28 October 1996; accepted 11 June 1997

Altered Neural Cell Fates and Medulloblastoma in Mouse *patched* Mutants

Lisa V. Goodrich, Ljiljana Milenković, Kay M. Higgins, Matthew P. Scott*

The *PATCHED* (*PTC*) gene encodes a Sonic hedgehog (Shh) receptor and a tumor suppressor protein that is defective in basal cell nevus syndrome (BCNS). Functions of *PTC* were investigated by inactivating the mouse gene. Mice homozygous for the *ptc* mutation died during embryogenesis and were found to have open and overgrown neural tubes. Two Shh target genes, *ptc* itself and *Gli*, were derepressed in the ectoderm and mesoderm but not in the endoderm. Shh targets that are, under normal conditions, transcribed ventrally were aberrantly expressed in dorsal and lateral neural tube cells. Thus Ptc appears to be essential for repression of genes that are locally activated by Shh. Mice heterozygous for the *ptc* mutation were larger than normal, and a subset of them developed hindlimb defects or cerebellar medulloblastomas, abnormalities also seen in BCNS patients.

The human *PTC* gene is a tumor suppressor and developmental regulator (*1*). Some patients with BCNS have germline mutations in *PTC* and are at increased risk for developmental defects such as spina bifida and craniofacial abnormalities, basal cell carcinoma of the skin, and brain tumors (*2*). *PTC* mutations also occur in sporadic basal cell carcinomas (*1*), which generally have both copies of *PTC* inactivated.

In the fruit fly *Drosophila*, Ptc is a key component of the Hedgehog (Hh) signaling pathway, which controls cell fate determination during development (*3*). Hh protein, secreted from localized regions, antagonizes the actions of its apparent receptor, Ptc, in nearby cells (*4*). In the absence of a Hh signal, Ptc represses transcription of multiple target genes, including *ptc* itself, *wingless* (a *Wnt* gene), and the *transforming growth factor* β–related gene *decapentaplegic*. In flies, *ptc* mutations cause derepression of target genes, cell fate changes, and excessive growth in some tissues (*5*). Hh induces a high level of *ptc* transcription by inhibiting the function of Ptc protein, so paradoxically an abundance of *ptc* transcript is an indicator of a low level of Ptc function. Vertebrate *ptc* expression is also regulated by Hh proteins (*6*), which can bind directly to Ptc (*7*).

The role of the Hh-Ptc pathway in skin cancer has been established by BCNS studies and with a mouse model (*8*), but less is known about the brain tumors associated with BCNS. About 3% of BCNS patients develop medulloblastomas (*9*), cerebellar tumors that usually arise in young children and have a mortality rate of ~50% (*10*). *ptc* mutations have been detected in sporadic medulloblastomas (*11*), but this tumor type is rare and there are few clear animal models (*12*), so much remains to be learned about its origins and biology.

To study the roles of *ptc* in development and in tumorigenesis, we constructed mice

Departments of Developmental Biology and Genetics and the Howard Hughes Medical Institute, Stanford University School of Medicine, Stanford, CA 94305–5427, USA.

*To whom correspondence should be addressed. E-mail: scott@cmgm.stanford.edu

lacking *ptc* function. By homologous recombination, part of *ptc* exon 1 (including the putative start codon) and all of exon 2 were replaced with *lacZ* and a neomycin resistance gene (Fig. 1) (*13*). Protein made from any alternative ATG codon would lack the first proposed transmembrane domain, flipping the orientation of the protein in the membrane. Three independent embryonic stem cell clones were used to make chimeras that were bred to B6D2F1 animals to generate heterozygous mice on a mixed background. Interbreeding of heterozygotes produced no homozygous animals among 202 offspring examined. Analysis of embryos from timed matings suggested that $ptc^{-/-}$ embryos die between embryonic day (E) 9.0 and E10.5, with the first gross phenotypes appearing by E8. In $ptc^{-/-}$ embryos, the neural tube failed to close completely and was overgrown in the head folds, hindbrain, and spinal cord (Fig. 2, A to C). Embryonic lethality may have been due to abnormal development of the heart (Fig. 2B).

In *Drosophila* Ptc protein inhibits *ptc* transcription. By inhibiting Ptc function, Hh increases production of Ptc, which may then bind available Hh and limit the range or duration of effective Hh signal (*14*). Hh signaling also posttranscriptionally regulates the zinc finger protein cubitus interruptus (ci) (*15*). In vertebrates, Sonic hedgehog (Shh) signaling induces transcription of both *ptc* and a *ci* homolog, *Gli* (*6*, *16*). Derepression of *ptc* and *Gli* in $ptc^{-/-}$ mice should therefore reveal where Ptc is normally active.

The expression of *ptc* and *Gli* was greatly increased in $ptc^{-/-}$ embryos. In $ptc^{+/-}$ mice, expression of the *lacZ* gene fused to the first *ptc* exon during targeting accurately reported the pattern of *ptc* transcription (Fig. 2, C and D). In $ptc^{-/-}$ embryos, expression of *ptc-lacZ* was extensively derepressed starting at about E8.0 in the anterior neural tube and spreading posteriorly by E8.75 (Fig. 2, C and E). Derepression was germ layer–specific: both *ptc-lacZ* and *Gli* were expressed throughout the ectoderm and mesoderm, but not in the endoderm (Fig. 2, D to G). *ptc* expression may be excluded from the endoderm so that Shh can signal the endoderm to the mesoderm (*17*). A differential requirement for Ptc may distinguish the germ layers.

As revealed by *ptc* mutants, an early site of Ptc activity is the neural tube, where Shh and Ptc act antagonistically to determine cell fates. Shh induces the floor plate and motor neurons in the ventral neural tube (*18*). These cell types fail to form in *Shh* mutants (*19*). Large amounts of Shh produced by the notochord may induce floor plate by completely inactivating Ptc (*18*). If so, elimination of *ptc* function might cause floor plate differentiation throughout the neural tube. Prospective floor plate cells transcribe the forkhead transcription factor *HNF3β* first and then *Shh* itself (*18*). In E8.5 *ptc* mutants, transcription of *HNF3β* and *Shh* was expanded dorsally (Fig. 3, A to C). Ectopic *Shh* expression was most extensive in the anterior, where transcripts could be detected throughout the neurepithelium (Fig. 3, B and C). Cells in this region were in a single layer with basal nuclei, like floor plate cells that are normally restricted to the ventral midline (Fig. 3, D and E). Expression of the lateral neural tube marker *Pax6* (*20*) was completely absent from *ptc* mutant embryos, suggesting that only ventral, and not ventrolateral, cell fates are specified (Fig. 3, F and G).

In principle, dorsalizing signals from the surface ectoderm (*21*) could confer dorsal cell fates even in the absence of *ptc* function. In E8-E9 *ptc* homozygotes, the dorsal neural tube marker *Pax3* was not expressed in the anterior neural tube but was transcribed in a very small region at the dorsalmost edge of the posterior neural tube (Fig. 3, H to J). In addition, *erb-b3* transcription, which marks migratory neural crest cells (Fig. 3K) (*22*), was not detected in the somites of *ptc* mutants (Fig. 3L). We conclude that only limited dorsal fate determination occurs in the absence of *ptc*. Bone morphogenetic protein (BMP) signals appear to maintain dorsal gene expression (*21*) so either *ptc* is required for BMPs to work or BMP signaling is ineffective in most cells expressing Shh targets.

Ventralization of the neural tube in *ptc* mutants occurred without affecting cell identity along the rostrocaudal axis. In $ptc^{-/-}$ embryos, cells in the anterior neural tube expressed the forebrain marker *Nkx2.1* (*23*), and cells in the spinal cord transcribed *hoxb1* (*24*) (Fig. 3, M and N). *hoxb1* was not transcribed in the fourth rhombomere of *ptc* mutants (Fig. 3N). This may reflect a transformation of hind-

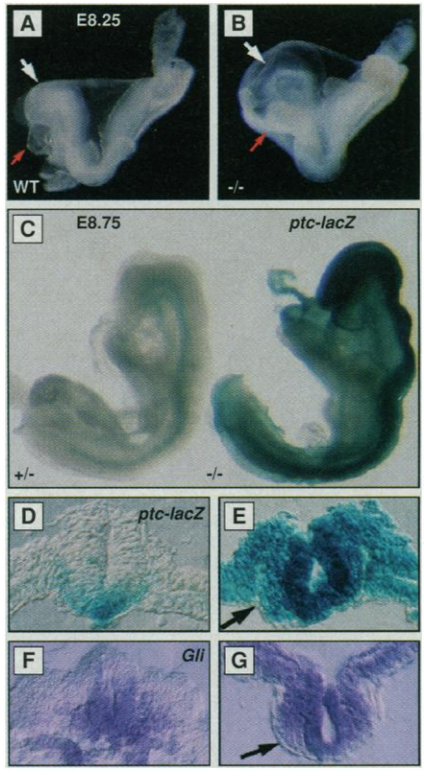

Fig. 2. Germ layer–specific derepression of Shh target genes in $ptc^{-/-}$ embryos. (**A** and **B**) Lateral views of E8.25 wild-type (WT) (A) and $ptc^{-/-}$ (B) embryos. The headfolds are overgrown in the mutant (white arrows) and the heart is not properly formed (red arrows). (**C**) Lateral views of E8.75 $ptc^{+/-}$ and $ptc^{-/-}$ embryos stained with X-Gal (*28*). (**D** through **G**) Transverse sections through E8.75 $ptc^{+/-}$ (D and F) and $ptc^{-/-}$ (E and G) embryos stained with X-Gal (D and E) or hybridized with a digoxigenin-labeled *Gli* probe (*29*) (F and G). Both *lacZ* and *Gli* were derepressed in the ectoderm and mesoderm but not in the endoderm (arrows). In (A) and (B), anterior is to the left and dorsal is up. In (C), anterior is up and dorsal is to the right. In (D) to (G), dorsal is up. Magnifications: (A) and (B), ~×16; (C), ~×20; (D) to (G), ~×125.

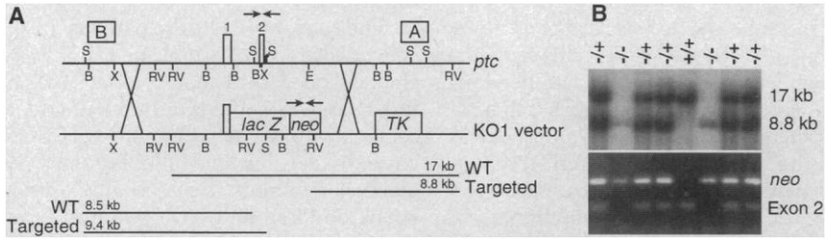

Fig. 1. Generation of the *ptc* mutation. (**A**) The *ptc* mutant allele was generated by homologous recombination between the KO1 targeting vector and *ptc*. External probe A detected a 3′ Eco RV polymorphism on blots and probe B detected a 5′ Sac I polymorphism. Exons are numbered. B, Bam HI; E, Eco RI; RV, Eco RV; S, Sac I; X, Xho I; *neo*, neomycin resistance gene; *TK*, thymidine kinase gene; WT, wild type. (**B**) Transmission of the *ptc* allele through the germ line was confirmed by Southern blot (upper panel) and a PCR genotyping assay (lower panel). PCR primers are indicated as arrows in (A). Because the homozygous mutant embryos were being resorbed, there was much less yolk sac DNA in the −/− lanes.

brain cells to floor plate, because *hoxb1* is excluded from the midline of wild-type embryos. Conversely, in the anterior, *Nkx2.1* expression was expanded dorsally in mutants compared with wild-type embryos (Fig. 3M).

The $ptc^{+/-}$ mice had features in common with BCNS patients: the mice were larger than their wild-type littermates [30.72 ± 3.83 g (average ± SD; $n = 29$) compared with 26.54 ± 2.51 g ($n = 39$) at 2 to 3 months; $P = 0.000001$ by t test], a small fraction (3 of 389 mice examined) had hindlimb defects such as extra digits or syndactyly (Fig. 4A) or obvious soft tissue tumors (1 of 243), and many developed brain tumors.

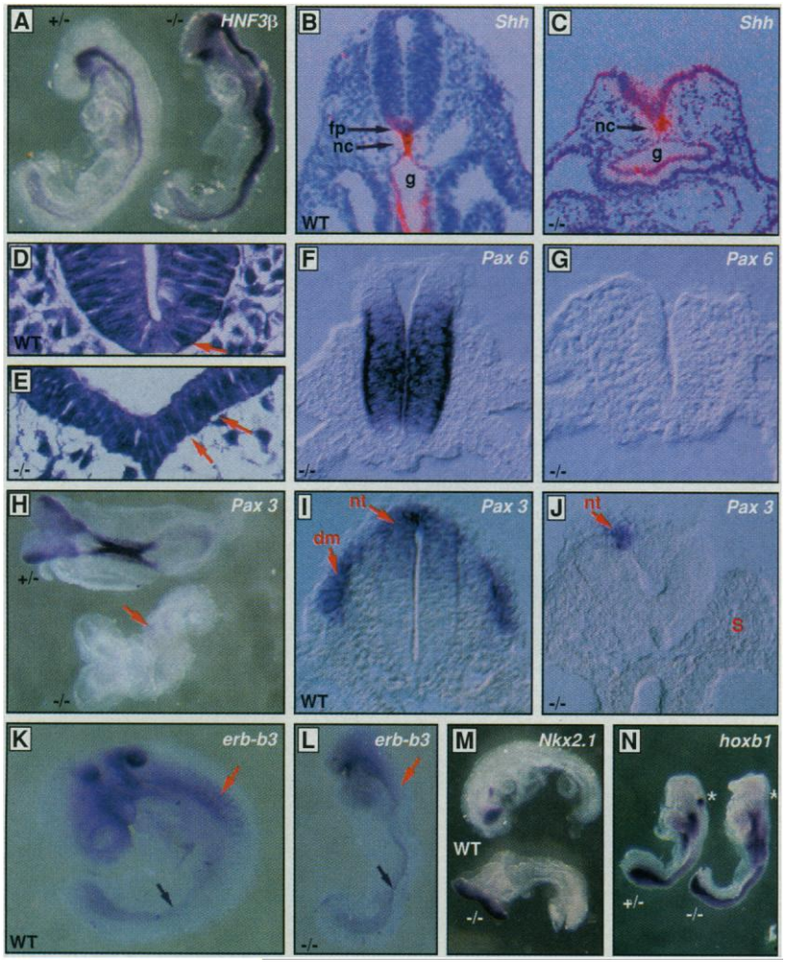

Fig. 3. Ventralization of the neural tube in $ptc^{-/-}$ embryos. (**A**) Lateral view of E8.5 $ptc^{+/-}$ and $ptc^{-/-}$ embryos hybridized with a *HNF3β* probe. Expression is expanded dorsally in the mutant. (**B** and **C**) Transverse sections through the hindbrain of E8.5 wild-type (B) and $ptc^{-/-}$ (C) embryos hybridized with ^{35}S-labeled *Shh* probe (*8*). *Shh* is expressed in the floor plate (fp) and notochord (nc) of the wild-type embryo and is greatly expanded in the *ptc* mutant. g, gut. (**D** and **E**) Hematoxylin and eosin stained transverse sections through the hindbrain of wild-type (D) and $ptc^{-/-}$ (E) E8.5 embryos. Bottle-shaped cells with basal nuclei are indicated by arrows. (**F** and **G**) Transverse sections through E8.5 wild type (F) and $ptc^{-/-}$ (G) embryos hybridized with a *Pax6* probe show the absence of expression in the $ptc^{+/-}$ mutant. (**H**) Dorsal view of E8.25 to E8.5 embryos hybridized with a *Pax3* probe. Because of the kinking in the neural tube, the $ptc^{-/-}$ embryo is curled on itself. Weak *Pax3* expression is seen in the posterior dorsal neural tube of the $ptc^{-/-}$ embryo (bottom, arrow). (**I** and **J**) Transverse sections through E8.5 wild-type (I) and $ptc^{-/-}$ (J) embryos hybridized with a *Pax3* probe. *Pax3* is expressed in the dorsal neural tube (nt) and dermamyotome (dm) in the wild-type but is present only in a small dorsal domain of the mutant neural tube; s, somite. (**K** and **L**) Lateral views of E9 wild-type (K) and E8.5 $ptc^{-/-}$ (L) embryos hybridized with an *erb-b3* probe. Staining is seen in migrating neural crest in the head and somites of wild type but not mutant embryos (red arrows). Weak staining in the head, heart, and gut (black arrows) is background or non–neural crest related. (**M**) Lateral view of wild-type (top) and $ptc^{-/-}$ (bottom) embryos hybridized with an *Nkx2.1* probe. The body of the mutant is twisted. *Nkx2.1* expression is limited to the anterior but is expanded dorsally in the mutant. (**N**) Lateral view of E8.5 $ptc^{+/-}$ and $ptc^{-/-}$ embryos hybridized with a *hoxb1* probe. Loss of expression in rhombomere four is indicated by the asterisks. In all transverse sections, dorsal is up. In (A), (K), (L), and (N), anterior is up and dorsal is to the right. In (H) and (M), anterior is to the left. Magnifications: (A), (H), (K), and (L), ~×16; (B) and (C), ~×100; (D) and (E), ~×364; (F), (G), (I), and (J), ~×160; (M) and (N), ~×11.

Of 243 $ptc^{+/-}$ mice that were between the ages of 2 and 9 months and were not killed for other studies, 18 died or were killed because of sickness. No wild-type littermates died. Ten of the affected heterozygotes were autopsied, and eight were found to have large growths in the cerebellum that resembled medulloblastomas (Fig. 4, B and C). Human medulloblastomas are believed to arise from a "primitive neurectodermal" cell type (*25*). They are most common in children, can be metastatic or nonmetastatic, and can have glial and neuronal properties. The histology of tumors from $ptc^{+/-}$ mice was similar to that of human medulloblastoma: tumor cells were small, with dark carrot-shaped nuclei and little cytoplasm (Fig. 4, D and E), and although a subset expressed neurofilament protein and synaptophysin (Fig. 4F) (*26*), the majority of cells appeared undifferentiated. Of the two autopsied animals without apparent medulloblastomas, one had a large tumor growing out of its rib muscle and the other died for unknown reasons. Medulloblastomas and soft tissue tumors were also observed in $ptc^{+/-}$ mice maintained on an inbred 129SV background: 6 of 27 had obvious medulloblastomas, 2 of 27 had soft tissue tumors, and 3 of 27 died but were not examined.

The *ptc* and *Gli* genes were strongly transcribed in the brain tumors but not in surrounding tissue (Fig. 5, A and B; $n = 3$ of three tumors examined). There was no detectable increase in *Shh* expression (Fig. 5C). To assess the incidence of medulloblastomas, brains from 47 asymptomatic $ptc^{+/-}$ mice were randomly collected and stained with X-Gal. Nine brains contained medulloblastomas that were easily recognized by their disorganized morphology and intense *ptc-lacZ* expression (Fig. 5D). Medulloblastomas were observed in 1 of 12 (8.3%) $ptc^{+/-}$ mice at 5 weeks of age, 1 of 12 (8.3%) mice at 9 to 10 weeks, and 7 of 23 (30.4%) mice at 12 to 25 weeks. Tumors can therefore arise as early as 5 weeks after birth but increase in severity and frequency as the animal ages.

We looked for changes in *ptc-lacZ* expression that might reflect early stages of tumorigenesis. At all stages examined, about half of the animals [50% at 5 to 10 weeks ($n = 24$), 56.5% at 12 to 25 weeks ($n = 23$)] exhibited regions of increased X-Gal staining on the surface of the cerebellum (Fig. 5E). These regions were usually lateral and often extended down into the fissures separating the folia (Fig. 5, E and F). The mouse medulloblastomas may arise

from these cells, which are superficial to the molecular layer of the cerebellum (Fig. 5F). During fetal development, prospective cerebellar granule cells proliferate in the external granule layer (EGL), the outermost layer of the cerebellum. Granule cells then leave and migrate past the Purkinje cells to form the internal granule cell layer of the adult animal, gradually depleting the EGL. The remnants of the fetal EGL have been proposed to be a source of human medulloblastoma progenitors, a hypothesis consistent with the higher frequency of these tumors in children (*27*).

The abundance of cerebellar *ptc* transcripts was reduced by about 50% in the $ptc^{+/-}$ mice compared with wild-type littermates (Fig. 5G). This reduction could lead to ectopic expression of Shh target genes and to uncontrolled cell proliferation. Brain tumors might arise from Ptc haploinsufficiency alone, from additional mutations in the second *ptc* allele, or from a combination of *ptc* mutations with mutations in other tumor suppressor loci. We have not observed basal cell carcinomas in $ptc^{+/-}$ mice, perhaps because somatic inactivation of the second *ptc* gene is required as it is in human basal cell carcinomas.

Our analysis has revealed that Ptc controls growth and pattern formation in early neural development and in the adult cerebellum. Autoregulation of *ptc* occurs in vertebrates as it does in *Drosophila*, and the balance between Hh and Ptc activities appears critical for normal development. The importance of Ptc dosage is emphasized by the phenotype of the $ptc^{+/-}$ mice, which develop a tumor type observed in the corresponding human cancer predisposition syndrome. Medulloblastoma is a common childhood brain tumor and the prognosis remains grim. The Hh-Ptc pathway may provide new diagnostic tools and new insights into tumorigenesis that can be directed toward potential therapies.

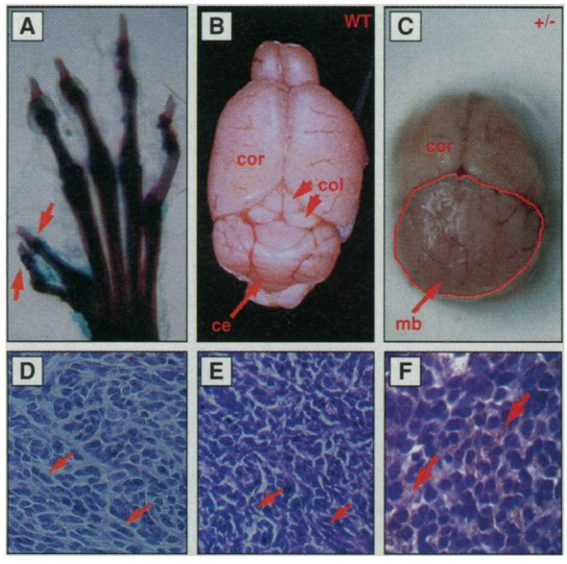

Fig. 4. Skeletal abnormalities and medulloblastomas in $ptc^{+/-}$ mice. (**A**) Alcian blue and Alizarin red stained hindlimb from a $ptc^{+/-}$ mouse (*30*). The preaxial digit is duplicated (arrows). (**B** and **C**) Dorsal views of brains from wild-type (B) and $ptc^{+/-}$ (C) mice. Anterior is up. In the posterior wild-type brain, the colliculi (col) are present as distinct bumps between the cortex (cor) and cerebellum (ce). In the $ptc^{+/-}$ mouse, a massive medulloblastoma (mb, outlined in red) grew over the colliculi and normal cerebellum, which can no longer be seen. The olfactory bulbs were removed. (**D** and **E**) Hematoxylin- and eosin-stained section through human (D) and mouse (E) medulloblastomas. The tumor cells are small with dark, carrot-shaped nuclei (arrows) and form nodules with no apparent orientation. (**F**) Synaptophysin immunoreactivity in a mouse medulloblastoma (*26*). Synaptophysin staining (brown) is seen in some processes (arrows). Nuclei are purple. Magnifications: (D) and (E), ~×300; (F), ~×500.

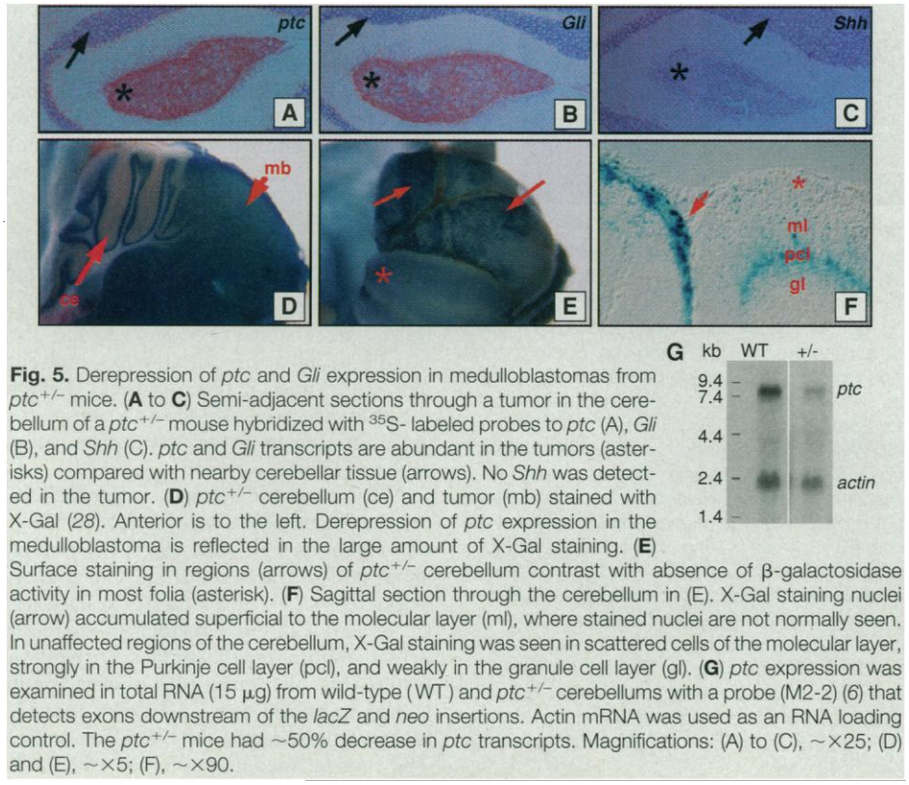

Fig. 5. Derepression of *ptc* and *Gli* expression in medulloblastomas from $ptc^{+/-}$ mice. (**A** to **C**) Semi-adjacent sections through a tumor in the cerebellum of a $ptc^{+/-}$ mouse hybridized with ^{35}S- labeled probes to *ptc* (A), *Gli* (B), and *Shh* (C). *ptc* and *Gli* transcripts are abundant in the tumors (asterisks) compared with nearby cerebellar tissue (arrows). No *Shh* was detected in the tumor. (**D**) $ptc^{+/-}$ cerebellum (ce) and tumor (mb) stained with X-Gal (*28*). Anterior is to the left. Derepression of *ptc* expression in the medulloblastoma is reflected in the large amount of X-Gal staining. (**E**) Surface staining in regions (arrows) of $ptc^{+/-}$ cerebellum contrast with absence of β-galactosidase activity in most folia (asterisk). (**F**) Sagittal section through the cerebellum in (E). X-Gal staining nuclei (arrow) accumulated superficial to the molecular layer (ml), where stained nuclei are not normally seen. In unaffected regions of the cerebellum, X-Gal staining was seen in scattered cells of the molecular layer, strongly in the Purkinje cell layer (pcl), and weakly in the granule cell layer (gl). (**G**) *ptc* expression was examined in total RNA (15 μg) from wild-type (WT) and $ptc^{+/-}$ cerebellums with a probe (M2-2) (*6*) that detects exons downstream of the *lacZ* and *neo* insertions. Actin mRNA was used as an RNA loading control. The $ptc^{+/-}$ mice had ~50% decrease in *ptc* transcripts. Magnifications: (A) to (C), ~×25; (D) and (E), ~×5; (F), ~×90.

REFERENCES AND NOTES

1. H. Hahn *et al.*, *Cell* **85**, 841 (1996); R. L. Johnson *et al.*, *Science* **272**, 1668 (1996).
2. R. J. Gorlin, *Medicine* **66**, 98 (1987).
3. M. Hammerschmidt, A. Brook, A. P. McMahon, *Trends Genet.* **13**, 14 (1997).
4. P. W. Ingham, A. M. Taylor, Y. Nakano, *Nature* **353**, 184 (1991).
5. P. W. Ingham, *Curr. Biol.* **4**, 347 (1994).
6. L. V. Goodrich, R. L. Johnson, L. Milenkovic, J. McMahon, M. P. Scott, *Genes Dev.* **10**, 301 (1996); V. Marigo, M. P. Scott, R. L. Johnson, L. Goodrich, C. J. Tabin, *Development* **122**, 1225 (1996); J.-P. Concordet *et al.*, *ibid.*, p. 2835.
7. V. Marigo *et al.*, *Nature* **384**, 176 (1996); D. M. Stone *et al.*, *ibid.*, p. 129.
8. A. E. Oro *et al.*, *Science* **276**, 817 (1997).
9. D. Lacombe, J. F. Chateil, D. Fontan, J. Battin, *Genet. Couns.* **1**, 273 (1990).
10. B. Novakovic, *Med. Pediatr. Oncol.* **23**, 480 (1994).
11. C. Raffel *et al.*, *Cancer Res.* **57**, 842 (1997); J. Xie *et al.*, *ibid.*, p. 2369.
12. K. M. Fung and J. Q. Trojanowski, *J. Neuropathol. Exp. Neurol.* **54**, 285 (1995); L. B. Rorke, *Am. J. Pathol.* **144**, 444 (1994).
13. DNA from the *ptc* genomic locus was isolated from a 129SV genomic phage library (Stratagene). Exons 1 through 15 of human *PTC* (*1*) were mapped by polymerase chain reaction (PCR) and sequencing. The 3′ arm of homology was a 3.5-kb Eco RI–Bam HI fragment from the second intron that gained a Bam HI site from pBSII (Stratagene) and was cloned into the Bam HI site of pPNT [V. L. Tybulewicz, C. E. Crawford, P. K. Jackson, R. T. Bronson, R. C. Mulligan, *Cell* **65**, 1153 (1991)]. A cassette containing the gene for nuclear localized β-galactosidase (*lacZ*) followed by the mP1 intron and poladenylate tail was excised from pNLacF [E. H. Mercer, G. W. Hoyle, R. P. Kapur, R. L. Brinster, R. D. Palmiter, *Neuron* **7**, 703 (1991)] and cloned into the Xho I site of pPNT by using Xho I and Sal I linkers. The 5′ arm of homology was a 6.5-kb Xho I–Nru I fragment that was cloned into the Xho I site upstream of *lacZ* with a Sal I linker.

The Nru I site is in the first *ptc* exon. The resulting plasmid, KO1, was linearized with Xho I and electroporated into RI embryonic stem cells that were subjected to double selection and analyzed by Southern (DNA) blot [A. L. Joyner, *Gene Targeting: A Practical Approach* (Oxford Univ. Press, New York, 1993), pp. 33–61]. Targeted clones were expanded and used for injection into C57Bl/6 blastocysts [B. Hogan, R. Beddington, F. Costantini, E. Lacy, *Manipulating the Mouse Embryo: A Laboratory Manual* (Cold Spring Harbor Laboratory Press, Cold Spring Harbor, NY, 1994), pp. 196–204].
14. Y. Chen and G. Struhl, *Cell* **87**, 553 (1996).
15. C. K. Motzny and R. Holmgren, *Mech. Dev.* **52**, 137 (1995); M. Domínguez, M. Brunner, E. Hafen, K. Basler, *Science* **272**, 1621 (1996); J. Hepker, Q. T. Wang, C. K. Motzny, R. Holmgren, T. V. Orenic, *Development* **124**, 549 (1997); P. Aza-Blanc, F.-A. Ramírez-Weber, M.-P. Laget, C. Schwartz, T. B. Kornberg, *Cell* **89**, 1043 (1997).
16. V. Marigo *et al.*, *Dev. Biol.* **180**, 273 (1996).
17. D. J. Roberts *et al.*, *Development* **121**, 3163 (1995).
18. Y. Echelard *et al.*, *Cell* **75**, 1417 (1993); H. Roelink *et al.*, *ibid.* **76**, 761 (1994); H. Roelink *et al.*, *ibid.* **81**, 445 (1995).
19. C. Chiang *et al.*, *Nature* **383**, 407 (1996).
20. C. Walther and P. Gruss, *Development* **113**, 1435 (1991).
21. M. E. Dickinson *et al.*, *ibid.* **121**, 2099 (1995); K. Liem Jr., G. Tremml, H. Roelink, T. M. Jessell, *Cell* **82**, 969 (1995).
22. H. U. Wang and D. J. Anderson, *Neuron* **18**, 383 (1997).
23. K. Shimamura *et al.*, *Development* **121**, 3923 (1995).
24. D. G. Wilkinson *et al.*, *Nature* **341**, 405 (1989).
25. J. P. Provias and L. E. Becker, *J. Neurooncol.* **29**, 35 (1996).
26. For immunostaining, two tumors were fixed and embedded in paraffin. Tissue sections (4 μm thick) were cleared and dehydrated, treated with 3% hydrogen peroxide, and then treated with a dilution of 1:10 normal rabbit serum (Vector Laboratories). Antibody to synaptophysin (Boehringer-Mannheim) was used at a dilution of 1:5 and antibody to neurofilament protein (Dako) at 1:50. Antibody binding was visualized with a peroxidase Vectastain Elite ABC kit (Vector Laboratories). Nuclei were counterstained with hematoxylin. As with anti-synaptophysin staining, anti-neurofilament staining appeared in processes of the tumor cells.
27. L. Stevenson and F. Echlin, *Arch. Neurol. Psychiatry* **31**, 93 (1934); M. E. Kadin, L. J. Rubinstein, J. S. Nelson, *J. Neuropathol. Exp. Neurol.* **29**, 583 (1970).
28. Embryos were stained with X-Gal (5-bromo-4-chloro-3-indoxyl-β-D-galactopyranoside) [C. Bonnerot and J. Nicolas, in *Guide to Techniques in Mouse Development*, P. M. Wassarman and M. L. DePamphilis, Eds. (Academic Press, New York, 1993), p. 463] and then sectioned. For X-Gal staining of tumors in heterozygotes, cerebellums were dissected, cut into four pieces along the sagittal plane, fixed briefly in 4% paraformaldehyde, and then stained.
29. D. G. Wilkinson, in *In situ Hybridization: A Practical Approach*, D. G. Wilkinson, Ed. (Oxford Univ. Press, Oxford, 1992), pp. 75–83.
30. M. C. Green, *Ohio J. Sci.* **52**, 31 (1952).
31. We thank D. Kingsley, S. McConnell, and G. Barsh for help with this project; D. Horoupian for advice on medulloblastoma histology; D. Jung and N. Jiang for technical assistance; A. Oro for helpful discussions; K. Wharton and L. Havton for advice and tissue samples; D. Anderson, P. Gruss, R. Krumlauf, A. McMahon, A. Nagy, J. Rossant, J. Rubinstein, A. Simeone, and D. Wilkinson for research materials; and the Protein and Nucleic Acid facility at Stanford for DNA help. L.V.G. is supported by an Howard Hughes Medical Institute predoctoral fellowship. This research was supported by the Howard Hughes Medical Institute. Mouse work was done according to Animal Use Guidelines at Stanford University.

19 May 1997; accepted 15 July 1997

Epidermal Cell Differentiation in *Arabidopsis* Determined by a *Myb* Homolog, *CPC*

Takuji Wada,* Tatsuhiko Tachibana, Yoshiro Shimura,* Kiyotaka Okada†

The roots of plants normally carry small hairs arranged in a regular pattern. Transfer DNA–tagged lines of *Arabidopsis thaliana* included a mutant with few, randomly distributed root hairs. The mutated gene *CAPRICE* (*CPC*) encoded a protein with a Myb-like DNA binding domain typical of transcription factors involved in animal and plant development. Analysis in combination with other root hair mutations showed that *CPC* may work together with the *TTG* gene and upstream of the *GL2* gene. Transgenic plants overexpressing *CPC* had more root hairs and fewer trichomes than normal. Thus, the *CPC* gene determines the fate of epidermal cell differentiation in *Arabidopsis*.

The cellular organization of the primary root of *Arabidopsis thaliana* is relatively simple and invariant (*1*). During the maturation of the root epidermis in *A. thaliana*, each cell ultimately becomes either a root hair (trichoblast; which we shall hereafter term a root hair cell) or a hairless cell (atrichoblast) (*2*, *3*). This choice may be determined by the position of the cell relative to the underlying cortical cell layer. Epidermal cell files that make contact with two cortical cell files by lying over the junction between the two cortical cell files are root hair cells. Epidermal cells that contact only one cortical cell file are hairless cells. Primary roots in wild-type *Arabidopsis* normally have eight files of cortical cells (Fig. 1F). Root hairs are tip-growing, tubular-shaped outgrowths that help to anchor roots, interact with soil microorganisms, and assist in the uptake of water and nutrients. *TRANSPARENT TESTA GLABRA* (*TTG*) and *GLABRA2* (*GL2*) are genes that determine whether epidermal cells differentiate into root hair cells or hairless cells (*3*, *4*). In *ttg* and *gl2* mutants, all of the epidermal cell files differentiate into root hair cells independent of their position relative to the underlying cortical cells. The *GL2* gene encodes a homeodomain protein that is expressed preferentially in the differentiating hairless epidermal cells (*4*, *5*). Although the *TTG* gene has not been cloned yet, it is believed to encode a protein with a Myc-like domain or a protein positively regulating a Myc-like gene, because the phenotype of the *ttg* mutant can be complemented by introducing a maize Myc gene, *R*, into the mutant. When the *R* gene is overexpressed in a wild-type plant, all of the root epidermal cells differentiate into hairless cells (*3*, *6*). Thus, *TTG* and *GL2* may inhibit the differentiation of root epidermal cells into root hair cells.

From a T3 population of transfer DNA (T-DNA)–tagged lines (*7*), we isolated a mutant with fewer than normal root hairs, which we named *caprice* (*cpc*) for the irregular distribution of root hairs (Fig. 1B). *cpc* is a nuclear mutation, not allelic to other known mutations. Heterozygous plants show the wild-type phenotype. From a cross between heterozygotes, about one-fourth (67/324) of the offspring had few root hairs, which indicated that *cpc* is a single, recessive mutation. The number of root hairs in the primary root of the *cpc* mutant was about one-fourth of that of the wild type (Table 1). The morphology and size of the root hairs produced by the *cpc* mutant were indistinguishable from those of wild-type hairs. The addition of 1-aminocyclopropane-1-carboxylic acid (ACC), an ethylene precursor, at 5×10^{-6} M induced root hair production in *cpc* seedlings; however, the number of hairs was about 30% of that of the ACC-treated wild type, indicating that ethylene cannot rescue the phenotypic deficiency of the *cpc* mutant (*8*).

To examine how the CPC gene works in combination with the *GL2* and *TTG* genes, we analyzed the phenotype of double mutants (Table 1). The *cpc gl2* double mutant had about the same number of root hairs as the *gl2* mutant, showing the *gl2* mutation to

T. Wada and K. Okada, Division I of Gene Expression and Regulation, National Institute for Basic Biology, Okazaki, 444, Japan, and Department of Botany, Graduate School of Science, Kyoto University, Kyoto, 606-01, Japan.
T. Tachibana, Department of Botany, Graduate School of Science, Kyoto University, Kyoto, 606-01, Japan.
Y. Shimura, Division I of Gene Expression and Regulation, National Institute for Basic Biology, Okazaki, 444, Japan, and Department of Biophysics, Graduate School of Science, Kyoto University, Kyoto, 606-01, Japan.

*Present address: Biomolecular Engineering Research Institute, 6-2-3 Furuedai, Suita, Osaka, 565, Japan.
†To whom correspondence should be addressed at the Department of Botany, Graduate School of Science, Kyoto University, Kyoto, 606-01, Japan. E-mail: kiyo@ok-lab.bot.kyoto-u.ac.jp